



Defect-Mediated Spin Relaxation and Dephasing in Graphene

M. B. Lundeberg, R. Yang, J. Renard, and J. A. Folk*

Department of Physics and Astronomy, University of British Columbia, Vancouver, British Columbia, Canada V6T1Z4

(Received 6 November 2012; published 11 April 2013)

A principal motivation to develop graphene for future devices has been its promise for quantum spintronics. Hyperfine and spin-orbit interactions are expected to be negligible in single-layer graphene. Spin transport experiments, on the other hand, show that graphene's spin relaxation is orders of magnitude faster than predicted. We present a quantum interference measurement that disentangles sources of magnetic and nonmagnetic decoherence in graphene. Magnetic defects are shown to be the primary cause of spin relaxation, masking any potential effects of spin-orbit interaction.

DOI: [10.1103/PhysRevLett.110.156601](https://doi.org/10.1103/PhysRevLett.110.156601)

PACS numbers: 72.80.Vp, 72.25.Rb, 73.20.Fz, 73.23.-b

Spin lifetimes in graphene are remarkable in that they are unremarkable. The first measurements of electron spin relaxation found 100 ps lifetimes [1]—similar to what one might expect for conventional metals or semiconductors—and more recent measurements confirm that initial result [2,3]. These experimental values can be contrasted with much more favorable theoretical predictions: micro- or even milliseconds are expected [4], due to carbon's low atomic number (weak spin-orbit interaction) and the lack of nuclear spin in the predominant isotope (weak hyperfine interaction). These material properties make graphene an extremely promising material for classical or quantum spintronics [5], but potential applications await an understanding of the practical mechanisms of spin relaxation in the material.

The orders-of-magnitude disconnect between spin relaxation measurements and theory remains one of the most important puzzles in graphene research. Recent theoretical work has focused on finding a mechanism that would give rise to unexpectedly strong spin-orbit interactions, perhaps associated with random electric fields from the substrate or localized electric fields near adatoms or vacancies [4]. Another possibility is that the conduction electrons in graphene are strongly coupled to magnetic moments, but this explanation lacks a microscopic picture of where these moments arise. It is possible to *create* defects with a magnetic moment intentionally in graphene, for example, by ion bombardment [6,7], but it remains an open question whether paramagnetic defects that may be present in intrinsic (natural) graphene explain the dephasing rate that is observed at low temperatures.

Quantum interference is a powerful tool for studying charge and spin interactions of conduction electrons with their material host. Random lattice strains, trigonal warping, and atomic-scale disorder in graphene dephase the valley symmetry, and dynamic electron-electron interactions give rise to inelastic charge dephasing [8–14]. Recently it has become clear that additional interactions lead to an apparent saturation of dephasing at temperatures below a kelvin [12,15]. The precise mechanism has yet to

be determined, but two of the proposed mechanisms have a direct bearing on the mystery of graphene's fast spin relaxation: uniaxial spin-orbit interactions [16] or defects with a magnetic moment [15,17].

This Letter presents a quantum interference measurement that distinguishes magnetic and nonmagnetic dephasing mechanisms in graphene for the first time. We demonstrate that magnetic moments are indeed a significant source of orbital dephasing in graphene, and are the dominant mechanism for spin relaxation [1–3]; in addition, we find a nonmagnetic dephasing mechanism of similar strength, whose microscopic origin is yet to be determined.

Parameters associated with quantum interference can be extracted from a transport measurement in two ways. Universal conductance fluctuations (UCF) are seen when the phase coherence length is comparable to device dimensions [Figs. 1(a)–1(c)], and their statistics may be compared to theoretical predictions. Alternatively, the average low-field magnetoconductance may be fit to weak localization (WL) theory. From an experimental point of view, WL measurements are an easier way to extract a dephasing rate, and historically much more common, but it is difficult or impossible to distinguish different dephasing mechanisms solely from WL. This experiment combines UCF and WL measurements to separate and quantify the various sources of dephasing in graphene. We begin by discussing UCF.

A monolayer graphene device was exfoliated onto an SiO₂/Si wafer [Fig. 1(a)] and measured in a dilution refrigerator with a two-axis magnet. Conductance G was measured in a four-terminal configuration, as a function of gate voltage V_{BG} , in-plane and out-of-plane magnetic fields B_{\parallel} and B_{\perp} , and temperature T [Figs. 1(b) and 1(c)]. Similar results were found in a second cooldown (different cryostat) of the same device after an annealing step. Conductance fluctuation data for a narrow range of V_{BG} (carrier density $n_s \approx 2.2 \times 10^{12} \text{ cm}^{-2}$) were analyzed by their autocorrelation in perpendicular magnetic field, $f(\delta B)$ [Fig. 1(d)].

UCF are dephased by any degrees of freedom in a conduction electron's environment that change faster than

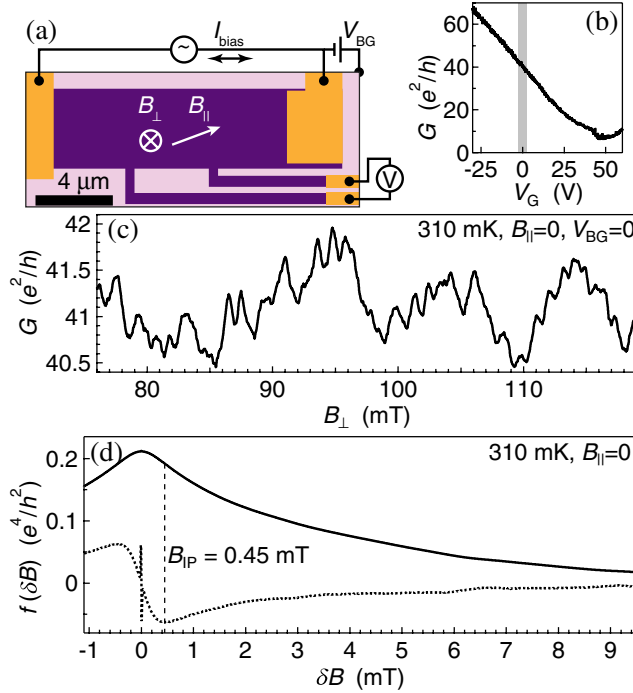


FIG. 1 (color online). (a) Simplified device geometry and measurement setup (see Supplemental Material [22] for device and measurement details). Dark purple regions are graphene, gold indicates leads, and light-shaded regions have been etched away. (b) Conductance as a function of gate voltage; the shaded region indicates the studied interval ($\epsilon_F \approx 200$ meV). (c) A typical UCF trace in perpendicular field. (d) A typical autocorrelation function (solid curve) and its derivative (dotted curve, no vertical scale plotted). The vertical spike in the dotted curve corresponds to the noise peak in the autocorrelation. The dashed line indicates the inflection point, used as a measure of coherence through Eq. (1).

the measurement bandwidth (hertz). The effective dephasing rate for UCF, τ_{UCF}^{-1} , is the sum of conduction electron scattering rates off of such dynamic centers [18,19]. This can be understood as an analog of the conventional effect of inelastic dephasing on WL, in which closed trajectories longer than the inelastic time do not contribute to coherent backscattering and therefore to the WL correction. For the case of UCF, quantum interference paths longer than the inelastic time do not contribute for similar reasons; in addition, paths long enough to include at least one dynamic scatterer—that is, a scatterer whose state changes faster than the measurement time scale—are averaged out and do not contribute to the measured conductance trace.

The dominant contributions to τ_{UCF}^{-1} at low temperatures are other conduction electrons, and dynamic defects in the device, whether magnetic or nonmagnetic. From an experimental point of view, the inflection point of $f(\delta B)$ provides a robust metric of this rate [20]:

$$\tau_{\text{UCF}}^{-1} \approx \frac{2eDB_{\text{IP}}}{3\hbar}, \quad \text{where} \quad \left. \frac{d^2 f}{d\delta B^2} \right|_{\delta B=B_{\text{IP}}} = 0, \quad (1)$$

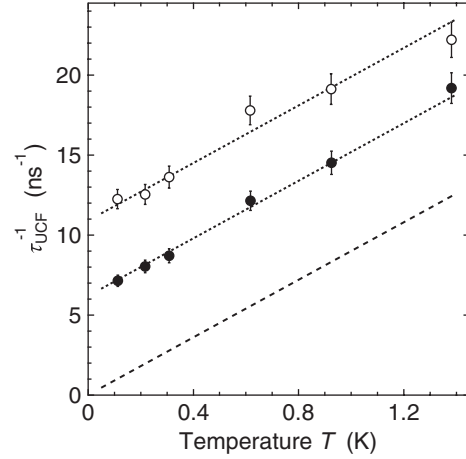


FIG. 2. Dependence of the rate τ_{UCF}^{-1} on temperature for $B_{\parallel} = 0$ (open circles) and $B_{\parallel} = 6$ T (filled circles). Dotted lines have slope $9.0 \text{ ns}^{-1}/\text{K}$ and offsets $\tau_{\text{UCF}}^{-1}(T=0) = 10.9 \text{ ns}^{-1}$ (upper line), $\tau_{\text{UCF}}^{-1}(T=0) = 6.2 \text{ ns}^{-1}$ (middle line). The lower, dashed line shows how τ_{UCF}^{-1} would appear without saturation [$\tau_{\text{UCF}}^{-1}(T=0) = 0$].

and $D = 0.03 \text{ m}^2/\text{s}$ is the diffusion constant that was calculated from G .

As seen in Fig. 2, the temperature dependence of τ_{UCF}^{-1} is linear over the range $T = 0.1, \dots, 1.4$ K with a slope that is close to the value predicted for electron-electron interactions [9,21] and an extrapolated offset $\tau_{\text{UCF}}^{-1}(T=0)$ that implies a low-temperature saturation of the dephasing rate [the corresponding length $\sqrt{D\tau_{\text{UCF}}(T=0)} = 1.7 \mu\text{m}$ is much smaller than the flake dimensions [Fig. 1(a)]]. Whereas certain symmetry-breaking static environments (e.g., out-of-plane spin-orbit coupling) can induce saturation in WL [15,16], they do not lead to a saturation in UCF [19,20]. Instead, the finite $\tau_{\text{UCF}}^{-1}(T=0)$ observed in this experiment indicates the presence of dynamic degenerate defects, that is, defects that do not freeze into a single state as temperature is decreased. The remainder of this work probes the nature of these degenerate defects: Are they magnetic, and how strongly do they interact with the conduction electrons (how fast do they change state)?

Performing the UCF measurement with an in-plane magnetic field shows clearly that some of the defects are magnetic: dephasing is reduced at $B_{\parallel} = 6$ T (Fig. 2), indicating that the magnetic moments have been polarized to a static configuration and no longer contribute to τ_{UCF}^{-1} . Quantitatively, the net change in τ_{UCF}^{-1} with large B_{\parallel} is the magnetic scattering rate: $\tau_{\text{mag}}^{-1} = 4.7 \pm 0.5 \text{ ns}^{-1}$ in Fig. 2. (The precise value of τ_{mag}^{-1} was seen to depend on sample details, for example, on carrier density; see Supplemental Material [22].)

The fast rate τ_{mag}^{-1} induced by magnetic defects is, in itself, an important finding, as it corresponds to the spin-flip rate for conduction electrons due to unpolarized magnetic defects [19]. The data in Fig. 2 therefore prove that magnetic defects induce sufficient spin relaxation to

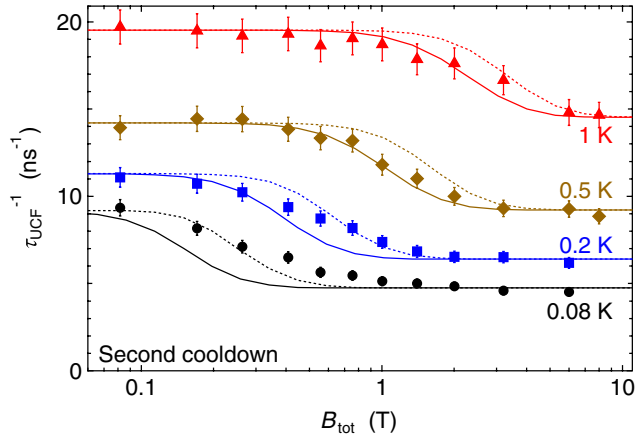


FIG. 3 (color online). Dependence of τ_{UCF}^{-1} on rms total magnetic field $B_{\text{tot}} = (B_{\parallel}^2 + B_{\perp}^2)^{1/2}$, for various T . Curves show the theoretical crossover for a scattering rate $\tau_{\text{mag}}^{-1} = 5 \text{ ns}^{-1}$ from spin- $\frac{1}{2}$ magnetic defects with $g = 2$ (solid lines) or $g = 1$ (dotted lines).

explain previous spin transport measurements in monolayer graphene [1–3].

The crossover to full defect polarization was analyzed in a second cooldown of this device (Fig. 3). The field required to turn off the dephasing grows with temperature, as expected for the thermodynamics of free magnetic moments. We obtain the theoretical curves in Fig. 3 by applying the definition of τ_{UCF}^{-1} in Eq. (1) to numerically simulated UCF with spin- $\frac{1}{2}$ defects (see Supplemental Material [22]). At high temperatures the behavior is consistent with defects of $g = 2$. A significant departure is seen at 200 mK and below, indicating the need for a more careful theoretical treatment of the magnetic defects as quantum objects [23,24].

The temperature dependence of the crossover in Fig. 3 eliminates any chance that our extracted τ_{mag}^{-1} might be associated with spin-orbit interaction. If the spin-orbit rate happened to be similar to τ_{UCF}^{-1} at a particular temperature, one could observe an inflated zero field τ_{UCF}^{-1} at that temperature [20], which would be reduced with B_{\parallel} . But such a coincidence would not occur over a wide range of temperature as observed experimentally. Furthermore, the magnitude of the drop (labeled τ_{mag}^{-1} in our analysis) would then depend strongly on temperature, contrary to the data.

The fact that $\tau_{\text{UCF}}^{-1}(T=0)$ does not go to zero at high field indicates an additional saturation mechanism that is apparently nonmagnetic, with dephasing rate $\tau_{\text{UCF}}^{-1}(T=0, B_{\parallel}=6\text{T}) \approx 6 \text{ ns}^{-1} (4 \text{ ns}^{-1})$ [Fig. 2 (Fig. 3) for the first (second) cooldown]. The data presented so far do not allow us to say more about this nonmagnetic mechanism. Is it merely device noise that limits UCF? Is it a more fundamental inelastic mechanism, such as the two-channel Kondo dephasing that was predicted for metals a decade ago [25]? Along the same lines, it is difficult to ascertain from the UCF data whether the magnetic dephasing results from a Kondo-type interaction of a few defect spins

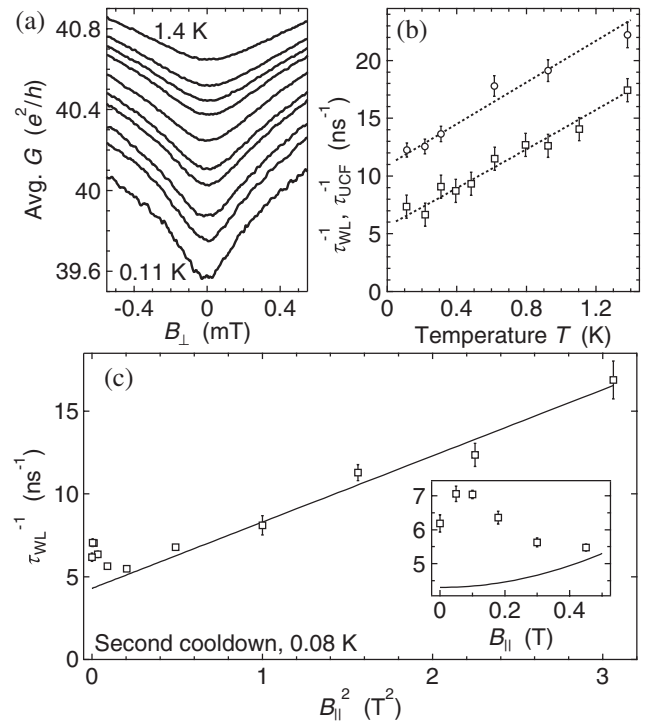


FIG. 4. (a) Conductance, averaged over the same V_{BG} range as used in Fig. 2. (b) Comparison of characteristic rates τ_{WL}^{-1} [square, extracted from (a)] and τ_{UCF}^{-1} (open circles, from Fig. 2) at $B_{\parallel} = 0$. The dotted lines are WL and UCF rates expected for electron-electron parameter $9.0 \text{ ns}^{-1}/\text{K}$, collision rate $\tau_{\text{mag}}^{-1} = 4.7 \text{ ns}^{-1}$ with slow magnetic defects, and nonmagnetic offsets of 3.5 ns^{-1} (WL), 6.2 ns^{-1} (UCF). (c) Dependence of τ_{WL}^{-1} on B_{\parallel}^2 (same V_{BG} range as used in Fig. 3). The solid line is $\tau_{\text{TRS}}^{-1}(B_{\parallel}) = 4.3 \text{ ns}^{-1} + (4.0 \text{ ns}^{-1}/\text{T}^2)B_{\parallel}^2$, a fit to the $B_{\parallel} \geq 1 \text{ T}$ data. Inset: The same data at low field, plotted linearly in B_{\parallel} .

strongly coupled to the electron gas, or from a large number of slowly fluctuating magnetic moments.

To address these questions we compare the UCF results to an analogous measurement based on WL, which is sensitive to time-reversal symmetry (TRS). Like UCF, WL may be dephased by a dynamic environment, but only when the fluctuations occur faster than the dephasing time scale—a cutoff time nine orders of magnitude shorter than the analogous time scale for UCF. Unlike UCF, WL is also dephased by a static environment if it does not preserve time-reversal symmetry; examples of this are magnetic fields or spin-flip processes from unpolarized magnetic moments.

Graphene’s magnetoconductance [Fig. 4(a)] is typically fit to a WL theory [8] that includes only nonmagnetic dephasing mechanisms, but the UCF data demonstrate that graphene also suffers from significant magnetic dephasing. If the magnetic defects vary slowly, they distinguish the spin-singlet and -triplet channels of the WL correction [18,19,26], which complicates the fitting. The dephasing can be more reliably characterized by

extracting the zero-field magnetoconductance curvature to obtain a single rate τ_{WL}^{-1} , defined as

$$\tau_{\text{WL}}^{-1} \equiv \frac{eD}{\hbar} \left(\frac{3\pi}{4} \frac{\hbar}{e^2} \frac{L}{W} \frac{d^2 \bar{G}}{dB_{\perp}^2} \Big|_{B_{\perp}=0} \right)^{-1/2}, \quad (2)$$

where $\frac{L}{W} = 1.05$ is the device aspect ratio and \bar{G} is the average conductance. For slow unpolarized magnetic defects ($B = 0$) [26], one expects

$$\tau_{\text{WL}}^{-1} \approx \left[\frac{3}{2} \left(\tau_{\text{TRS}}^{-1} + \frac{2}{3} \tau_{\text{mag}}^{-1} \right)^{-2} - \frac{1}{2} \left(\tau_{\text{TRS}}^{-1} + 2\tau_{\text{mag}}^{-1} \right)^{-2} \right]^{-1/2}, \quad (3)$$

where τ_{mag}^{-1} is defined the same as for UCF and τ_{TRS}^{-1} is the summed dephasing rate from other scattering mechanisms that break time-reversal symmetry. For fast magnetic defects, on the other hand, τ_{WL}^{-1} is simply the sum of rates $\approx \tau_{\text{TRS}}^{-1} + \tau_{\text{mag}}^{-1}$ [18].

As in the case of UCF, τ_{WL}^{-1} is seen to increase with temperature, and a zero-temperature offset is clearly observed [Fig. 4(b)]. The common slope with respect to T reflects the equal effect of electron-electron interactions on WL and UCF [21], thereby confirming that Eqs. (1) and (2) are not miscalibrated. The effect of an in-plane field on WL [Fig. 4(c)] is more complicated than the analogous measurement for UCF (Fig. 3) due to graphene's ripples, which convert the uniform in-plane field to a random vector potential. This breaks time-reversal symmetry [27,28], giving $\tau_{\text{TRS}}^{-1}(B_{\parallel}) = \tau_{\text{TRS}}^{-1}(0) + \beta B_{\parallel}^2$, where $\tau_{\text{TRS}}^{-1}(0)$ is the inelastic dephasing rate from nonmagnetic sources and β describes the ripple geometry.

In the data τ_{WL}^{-1} increases sharply from 0 to 50 mT, which can be explained by the suppression of two WL channels by Zeeman splitting and the resultant transition from Eq. (3) to $\tau_{\text{WL}}^{-1} = \tau_{\text{TRS}}^{-1} + \frac{2}{3} \tau_{\text{mag}}^{-1}$ [23]. Above 50 mT, τ_{WL}^{-1} decreases at first as the magnetic defects polarize and their dephasing effect vanishes. For much higher fields ($B_{\parallel} > 0.5$ T) the defects are fully polarized and τ_{WL}^{-1} has collapsed to τ_{TRS}^{-1} , giving the B_{\parallel}^2 dependence seen in Fig. 4(c).

Considering UCF and WL data together, we can draw several conclusions about the mechanisms of spin relaxation and low-temperature dephasing in graphene.

(1) Scattering from magnetic defects induces a spin-flip rate $\tau_{\text{mag}}^{-1} \approx 5 \text{ ns}^{-1}$ in the data presented. This is seen directly as the field-induced suppression of τ_{UCF}^{-1} (Fig. 3). The smaller field-induced suppression of τ_{WL}^{-1} [$\sim 2 \text{ ns}^{-1}$, Fig. 4(c)] is consistent with the weaker contribution of τ_{mag}^{-1} to τ_{WL}^{-1} for slow magnetic defects: those that change slowly on the dephasing time scale but fast enough to dephase UCF.

(2) Further evidence that spin relaxation from magnetic defects overwhelms any contribution from spin-orbit interaction can be found from the field dependence of τ_{WL}^{-1} . If spin-orbit interaction were dominant (either in plane or out of plane), the evolution of τ_{WL}^{-1} with B_{\parallel} would have been

qualitatively different from what is observed (see Supplemental Material [22]): a sharp *drop* at low field, followed by the steady rise due to ripples [16], rather than the sharp *rise* that is observed experimentally for low field, followed by a drop due to defect polarization, then the ripple-induced rise.

(3) The data in Fig. 4(c) can be explained quantitatively only by including an extra WL dephasing mechanism, in addition to the $\tau_{\text{mag}}^{-1} \approx 5 \text{ ns}^{-1}$ from defects and the expected $\tau_{\text{TRS}}^{-1} = 0.8 \text{ ns}^{-1}$ from electron-electron interactions. One possible mechanism is scattering from nonmagnetic impurities whose evolution is fast enough to break time-reversal symmetry, yielding an effective dephasing rate of 1.8 ns^{-1} . A second possibility is in-plane spin-orbit coupling, with magnitude up to $\tau_{\text{xy}}^{-1} = 2.6 \text{ ns}^{-1}$ including contributions along both in-plane directions. Either mechanism could explain the precise form of WL in-plane field dependence. Out-of-plane spin-orbit interaction, $\tau_z^{-1} = 3.3 \text{ ns}^{-1}$, would yield a field dependence that is qualitatively but not quantitatively consistent with the data. A more detailed comparison of these mechanisms with the data is found in the Supplemental Material [22].

Both magnetic and nonmagnetic dephasing mechanisms limit coherence in graphene below 1 K. The magnetic scattering rate is too large to be explained by remote magnetic moments, requiring instead that the magnetic defects are electronically coupled to the graphene. Recent WL data [15] suggest that the magnetic defects may be midgap states at the Dirac point, formed at vacancies or edges. For the nonmagnetic dephasing of UCF, and possibly also WL, we can rule out bistable charge systems in the SiO_2 substrate; their broadly distributed level splittings would produce a rate proportional to T [25]. The data instead suggest a class of nearly degenerate nonmagnetic defects in the graphene itself, whose microscopic origin is yet to be determined.

We acknowledge helpful discussions with V.I. Fal'ko. Graphite crystals were provided by D. Cobden. J.R. acknowledges funding from the CIFAR JF Academy and from the Max Planck-UBC Center for Quantum Materials. J.F. acknowledges support from the Alfred P. Sloan Foundation. This work was funded by CIFAR, CFI, and NSERC.

*jfolk@physics.ubc.ca

- [1] N. Tombros, C. Jozsa, M. Popinciuc, H. T. Jonkman, and B. J. van Wees, *Nature (London)* **448**, 571 (2007).
- [2] W. Han, K. Pi, K. M. McCreary, Y. Li, J. J. I. Wong, A. G. Swartz, and R. K. Kawakami, *Phys. Rev. Lett.* **105**, 167202 (2010).
- [3] W. Han and R. K. Kawakami, *Phys. Rev. Lett.* **107**, 047207 (2011).
- [4] C. Ertler, S. Konschuh, M. Gmitra, and J. Fabian, *Phys. Rev. B* **80**, 041405 (2009).

- [5] B. Trauzettel, D. V. Bulaev, D. Loss, and G. Burkard, *Nat. Phys.* **3**, 192 (2007).
- [6] R.R. Nair, M. Sepioni, I.-L. Tsai, O. Lehtinen, J. Keinonen, A.V. Krasheninnikov, T. Thomson, A.K. Geim, and I.V. Grigorieva, *Nat. Phys.* **8**, 199 (2012).
- [7] X. Hong, K. Zou, B. Wang, S.-H. Cheng, and J. Zhu, *Phys. Rev. Lett.* **108**, 226602 (2012).
- [8] E. McCann, K. Kechedzhi, V.I. Fal'ko, H. Suzuura, T. Ando, and B.L. Altshuler, *Phys. Rev. Lett.* **97**, 146805 (2006).
- [9] F.V. Tikhonenko, D.W. Horsell, R.V. Gorbachev, and A.K. Savchenko, *Phys. Rev. Lett.* **100**, 056802 (2008).
- [10] K. Kechedzhi, O. Kashuba, and V.I. Fal'ko, *Phys. Rev. B* **77**, 193403 (2008).
- [11] M.Y. Kharitonov and K.B. Efetov, *Phys. Rev. B* **78**, 033404 (2008).
- [12] D.-K. Ki, D. Jeong, J.-H. Choi, H.-J. Lee, and K.-S. Park, *Phys. Rev. B* **78**, 125409 (2008).
- [13] F.V. Tikhonenko, A.A. Kozikov, A.K. Savchenko, and R.V. Gorbachev, *Phys. Rev. Lett.* **103**, 226801 (2009).
- [14] S. Lara-Avila, A. Tzalenchuk, S. Kubatkin, R. Yakimova, T.J.B.M. Janssen, K. Cedergren, T. Bergsten, and V. Fal'ko, *Phys. Rev. Lett.* **107**, 166602 (2011).
- [15] A.A. Kozikov, D.W. Horsell, E. McCann, and V.I. Fal'ko, *Phys. Rev. B* **86**, 045436 (2012).
- [16] E. McCann and V.I. Fal'ko, *Phys. Rev. Lett.* **108**, 166606 (2012).
- [17] F. Pierre, A.B. Gougam, A. Anthore, H. Pothier, D. Esteve, and N.O. Birge, *Phys. Rev. B* **68**, 085413 (2003).
- [18] A.A. Bobkov, V.I. Fal'ko, and D.E. Khmel'nitskii, *Zh. Eksp. Teor. Fiz.* **98**, 703 (1990) [*Sov. Phys. JETP* **71**, 393 (1990)].
- [19] E. Akkermans and G. Montambaux, *Mesoscopic Physics of Electrons and Photons* (Cambridge University Press, Cambridge, England, 2007).
- [20] M.B. Lundeberg, J. Renard, and J.A. Folk, *Phys. Rev. B* **86**, 205413 (2012).
- [21] I.L. Aleiner and Y.M. Blanter, *Phys. Rev. B* **65**, 115317 (2002).
- [22] See Supplemental Material at <http://link.aps.org/supplemental/10.1103/PhysRevLett.110.156601> for sample details, checks for device overheating, the gate dependence of τ_{mag} , and theoretical discussions about the accuracy of Eq. (1) as well as the effects of Zeeman splitting and spin-orbit coupling.
- [23] M.G. Vavilov and L.I. Glazman, *Phys. Rev. B* **67**, 115310 (2003).
- [24] T. Micklitz, T.A. Costi, and A. Rosch, *Phys. Rev. B* **75**, 054406 (2007).
- [25] A. Zawadowski, J. von Delft, and D.C. Ralph, *Phys. Rev. Lett.* **83**, 2632 (1999).
- [26] S. Hikami, A.I. Larkin, and Y. Nagaoka, *Prog. Theor. Phys.* **63**, 707 (1980).
- [27] M.B. Lundeberg and J.A. Folk, *Phys. Rev. Lett.* **105**, 146804 (2010).
- [28] H. Mathur and H.U. Baranger, *Phys. Rev. B* **64**, 235325 (2001).